INTERNATIONAL JOURNAL FOR NUMERICAL METHODS IN FLUIDS
Int. J. Numer. Meth. Fluids 2006; **52**:941–962
Published online 15 March 2006 in Wiley InterScience (www.interscience.wiley.com). DOI: 10.1002/fld.1209

Comparison of GMRES and ORTHOMIN for the black oil model on unstructured grids

Wenjun Li[‡], Zhangxin Chen[*,†], Guanren Huan[§] and Xiuzhen Sun[¶]

Department of Mathematics, Southern Methodist University, Box 750156, Dallas, TX 75275-0156, U.S.A.

SUMMARY

This paper addresses an application of ORTHOMIN and GMRES to petroleum reservoir simulation using the black oil model on unstructured grids. Comparisons between these two algorithms are presented in terms of storage and total flops per restart step. Numerical results indicate that GMRES is faster than ORTHOMIN for all tested petroleum reservoir problems, particularly for large scale problems. The control volume function approximation method is utilized in the discretization of the governing equations of the black oil model. This method can accurately approximate both the pressure and velocity in the simulation of multiphase flow in porous media, effectively reduce grid orientation effects, and be easily applied to arbitrarily shaped control volumes. It is particularly suitable for hybrid grid reservoir simulation. Copyright © 2006 John Wiley & Sons, Ltd.

KEY WORDS: oil reservoir simulator; ORTHOMIN; GMRES; ILU preconditioner; control volume function approximation method; fully implicit scheme

1. INTRODUCTION

Nowadays, new requirements on petroleum reservoir simulation technology are very sophisticated. These requirements include fine unstructured grids for development of new oil/gas fields, management of old oil/gas fields, and shortening of history matching processes and simulation time, for example. On one hand, the fine unstructured grids easily generate a large-scale simulation model with a size of millions of unknowns. On the other hand, the shortening of history matching and simulation time requires fast and accurate algorithms for solving large-scale systems. Moreover, the systems of algebraic equations arising from the

[*]Correspondence to: Zhangxin Chen, Department of Mathematics, Southern Methodist University, Box 750156, Dallas, TX 75275-0156, U.S.A.
[†]E-mail: zchen@mail.smu.edu
[‡]E-mail: wli@mail.smu.edu
[§]E-mail: ghuan@mail.smu.edu
[¶]E-mail: xi-uzhens@mail.smu.edu

Received 23 March 2005
Revised 23 January 2006
Accepted 24 January 2006

numerical discretization of the governing equations for multiphase flow in reservoirs have special properties. The coefficient (stiffness) matrices of these systems are sparse but nonsymmetric and indefinite, for example. While sparse, their band structure is usually spoiled by wells that perforate into many gridblocks and by irregular gridblock structure. Furthermore, for petroleum simulation problems with a number of gridblocks of over 100 000, about 80–90% of the total simulation time is spent on solution of linear systems. Thus the choice of a linear solver is very important in the numerical simulation of multiphase flow.

To model accurately and efficiently irregularly geometrical and geological features and flow patterns of a reservoir, gridding techniques of unstructured girds and various discretization methods have been developed in the past decade [1]. Heinrichs [2] introduced the perpendicular bisector (PEBI) method, Forsyth [3] developed control volume finite element (CVFE) grids and the CVFE method for thermal reservoir simulation, and Fung *et al*. [4] applied them to commercial thermal reservoir simulators. Verma and Aziz [5] improved the CVFE method to deal with permeability tensors using three-dimensional CVFE grids. Li *et al*. [6] recently introduced the control volume function approximation (CVFA) method into the black oil reservoir simulation using arbitrarily shaped grids and checked the stability and accuracy of this method to deal with the 'bubble point' and coning problems [7]. Because the connection between grid blocks is irregular for unstructured grids, the Jacobian matrices for these grids are much more complicated than those for structured grids. Furthermore, the grid irregularity requires a great amount of memory and computational time to solve systems of algebraic equations. In this paper we apply the CVFA to discretize the governing equations of the black oil model. This method can directly discretize these equations on arbitrarily shaped control volumes and can guarantee that the flux is continuous across an interface between two neighbouring control volumes.

The orthogonal minimum residual (ORTHOMIN) algorithm [8] is capable of solving sparse, nonsymmetric systems of algebraic equations. It has been applied to petroleum reservoir simulation and is still widely used, particularly for reservoir simulation on structured grids. In this paper we study its application to unstructured reservoir simulation using the black oil model. Also, we discuss an application of the generalized minimum residual (GMRES) algorithm to unstructured grids. GMRES [9] is more efficient and robust, particularly for solution of large systems. This algorithm has been applied to numerical solution of the Navier–Stokes equations of compressible flow [10] and multiphase flow in porous media on structured grids [11]. Here we focus on its application to unstructured reservoir simulation. In addition, we carry out comparisons between these two algorithms in terms of storage, total flops per restart, and CPU time for benchmark problems of the comparative solution projects (CSP) organized by the society of petroleum engineers (SPE) and for real oil field problems. Numerical results indicate that GMRES is faster than ORTHOMIN for all tested petroleum reservoir problems, particularly for large scale problems. GMRES uses only as much as 61% of the CPU time of ORTHOMIN for some of the tested problems in this paper.

The rest of the paper is organized as follows. In the next section, we briefly review the black oil model, its linearization by the Newton–Raphson procedure, and its discretization by the CVFA. Then, in the third section, for the purpose of comparison we state ORTHOMIN and GMRES. Comparisons between these two algorithms in terms of their storage and flops are presented in the fourth section. In the last section we apply ORTHOMIN and GMRES to five simulation problems, compare them numerically, and make concluding remarks.

2. THE BLACK OIL MODEL AND ITS DISCRETIZATION

In the black oil model, it is assumed that the hydrocarbon components are divided into a gas component and an oil component in a stock tank at the standard pressure and temperature and that no mass transfer occurs between the water phase and the other two phases (oil and gas). The gas component mainly consists of methane and ethane.

Let ϕ and K denote the porosity and permeability of a porous medium $\Omega \subset \Re^3$, s_α, μ_α, p_α, $\mathbf{u}_\alpha$, B_α, and $K_{r\alpha}$ be the saturation, viscosity, pressure, volumetric velocity, formation volume factor, and relative permeability of the α phase, $\alpha = \mathrm{w}, \mathrm{o}, \mathrm{g}$, respectively, and R_{so} be the gas solubility. Then the mass conservation equations of the black oil model are [12, 13]

$$-\nabla \cdot \left(\frac{\rho_{\mathrm{WS}}}{B_{\mathrm{w}}} \mathbf{u}_{\mathrm{w}} \right) + q_{\mathrm{W}} = \frac{\partial}{\partial t} \left(\phi \frac{\rho_{\mathrm{WS}}}{B_{\mathrm{w}}} s_{\mathrm{w}} \right) \tag{1}$$

for the water component

$$-\nabla \cdot \left(\frac{\rho_{\mathrm{OS}}}{B_{\mathrm{o}}} \mathbf{u}_{\mathrm{o}} \right) + q_{\mathrm{O}} = \frac{\partial}{\partial t} \left(\phi \frac{\rho_{\mathrm{OS}}}{B_{\mathrm{o}}} s_{\mathrm{o}} \right) \tag{2}$$

for the oil component, and

$$-\nabla \cdot \left(\frac{\rho_{\mathrm{GS}}}{B_{\mathrm{g}}} \mathbf{u}_{\mathrm{g}} + \frac{R_{\mathrm{so}} \rho_{\mathrm{GS}}}{B_{\mathrm{o}}} \mathbf{u}_{\mathrm{o}} \right) + q_{\mathrm{G}} = \frac{\partial}{\partial t} \left[\phi \left(\frac{\rho_{\mathrm{GS}}}{B_{\mathrm{g}}} s_{\mathrm{g}} + \frac{R_{\mathrm{so}} \rho_{\mathrm{GS}}}{B_{\mathrm{o}}} s_{\mathrm{o}} \right) \right] \tag{3}$$

for the gas component, where $\rho_{\beta \mathrm{S}}$ is the density of the β component at standard conditions (stock tank), and q_β is the mass flow rate of component β at wells, $\beta = \mathrm{W}, \mathrm{O}, \mathrm{G}$. The volumetric velocity of the α phase is represented by Darcy's law

$$\mathbf{u}_\alpha = -\frac{K K_{r\alpha}}{\mu_\alpha} \nabla \Phi_\alpha, \quad \alpha = \mathrm{w}, \mathrm{o}, \mathrm{g} \tag{4}$$

where the potential Φ_α of the α phase is given by

$$\Phi_\alpha = p_\alpha - \rho_\alpha \tilde{g} D, \quad \alpha = \mathrm{w}, \mathrm{o}, \mathrm{g} \tag{5}$$

ρ_α represents the density of the α phase, $\tilde{g}$ is the gravitational constant, and D is the depth function. The saturations of the water, oil, and gas phases satisfy the constraint

$$s_{\mathrm{w}} + s_{\mathrm{o}} + s_{\mathrm{g}} = 1 \tag{6}$$

Furthermore, the phase pressures are related by the capillary pressures p_{cow} and p_{cgo}:

$$p_{\mathrm{cow}} = p_{\mathrm{o}} - p_{\mathrm{w}}, \quad p_{\mathrm{cgo}} = p_{\mathrm{g}} - p_{\mathrm{o}} \tag{7}$$

Finally, the mass flow rates q_β of wells can be calculated using Peaceman's formulas [13, 14].

The boundary and initial conditions are given as follows. In this paper we consider no flow boundary conditions

$$\mathbf{u}_\alpha \cdot \mathbf{n} = 0, \quad \alpha = \mathrm{w}, \mathrm{o}, \mathrm{g}, \quad \mathbf{x} \in \partial\Omega \tag{8}$$

where $\mathbf{n}$ is the outward unit norm to the boundary $\partial\Omega$ of the reservoir domain Ω. The initial conditions depend on the state of a reservoir. When all gas dissolves into the oil phase,

there is no gas phase present, i.e. $s_g = 0$. In such a case, the reservoir is said to be in the undersaturated state. If all three phases co-exist, the reservoir is referred to as in the saturated state. In the undersaturated state, we use $p = p_o$, s_w, and p_b as the unknowns, where p_b is the bubble point pressure; see Reference [7]. The corresponding initial conditions are

$$\begin{aligned} p(\mathbf{x},0) &= p^0(\mathbf{x}), \quad \mathbf{x} \in \Omega \\ s_w(\mathbf{x},0) &= s_w^0(\mathbf{x}), \quad \mathbf{x} \in \Omega \\ p_b(\mathbf{x},0) &= p_b^0(\mathbf{x}), \quad \mathbf{x} \in \Omega \end{aligned} \tag{9}$$

In the saturated state, we employ $p = p_o$, s_w, and s_o as the unknowns. In this case, the initial conditions become

$$\begin{aligned} p(\mathbf{x},0) &= p^0(\mathbf{x}), \quad \mathbf{x} \in \Omega \\ s_w(\mathbf{x},0) &= s_w^0(\mathbf{x}), \quad \mathbf{x} \in \Omega \\ s_o(\mathbf{x},0) &= s_o^0(\mathbf{x}), \quad \mathbf{x} \in \Omega \end{aligned} \tag{10}$$

We use a fully implicit method to solve the nonlinear equations (1)–(9) (or (10)) and apply the CVFA to discretize them in space. To model accurately the geometrical and geological features of a reservoir, a hybrid grid needs to be used for reservoir simulation. As noted, because the CVFA can directly discretize an equation on arbitrarily shaped grids and is especially suitable for hybrid grid reservoir simulation, we apply this method to the discretization of the governing equations of the black oil model and the treatment of wells.

We very briefly review the discretization of the black oil model using the CVFA and the linearization of this model using the Newton–Raphson iteration. For more details, refer to Reference [7]. Let V_i be a control volume. Substituting Equations (4) with $\alpha = \mathrm{w}, \mathrm{o}, \mathrm{g}$ into (1)–(3), respectively, and using the divergence theorem, the integral forms of the resulting equations are

$$\oint_{\partial V_i} \frac{\rho_{WS}}{B_w} \frac{KK_{rw}}{\mu_w} \nabla\Phi_w \cdot \mathbf{n}\, \mathrm{d}A + \int_{V_i} q_W\, \mathrm{d}V = \int_{V_i} \frac{\partial}{\partial t}\left(\phi \frac{\rho_{WS}}{B_w} s_w\right) \mathrm{d}V \tag{11}$$

for the water component

$$\oint_{\partial V_i} \frac{\rho_{OS}}{B_o} \frac{KK_{ro}}{\mu_o} \nabla\Phi_o \cdot \mathbf{n}\, \mathrm{d}A + \int_{V_i} q_O\, \mathrm{d}V = \int_{V_i} \frac{\partial}{\partial t}\left(\phi \frac{\rho_{OS}}{B_o} s_o\right) \mathrm{d}V \tag{12}$$

for the oil component, and

$$\begin{aligned} &\oint_{\partial V_i} \left(\frac{\rho_{GS}}{B_g} \frac{KK_{rg}}{\mu_g} \nabla\Phi_g + \frac{R_{so}\rho_{GS}}{B_o} \frac{KK_{ro}}{\mu_o} \nabla\Phi_o\right) \cdot \mathbf{n}\, \mathrm{d}A + \int_{V_i} q_G\, \mathrm{d}V \\ &\quad = \int_{V_i} \frac{\partial}{\partial t}\left[\phi\left(\frac{\rho_{GS}}{B_g} s_g + \frac{R_{so}\rho_{GS}}{B_o} s_o\right)\right] \mathrm{d}V \end{aligned} \tag{13}$$

for the gas component, where $\mathbf{n}$ is the outward unit norm to ∂V_i.

Since the unknowns on control volumes can be different under different states of a reservoir, the integral forms of the governing equations on each control volume are solved, respectively,

according to the undersaturated and saturated states. In the undersaturated state, the lth iteration values of the water and oil potentials on boundary e_{ij} of V_i at the $(n+1)$th time step are approximated by

$$\begin{aligned}(\Phi_{wh})_l^{(n+1)} &= \sum_{r=0}^{R_{ij}} (\Phi^i_{w_{j,r}})_l^{(n+1)} \phi^i_{j,r}(\mathbf{x}), \quad \mathbf{x} \in e_{ij} \\ (\Phi_{oh})_l^{(n+1)} &= \sum_{r=0}^{R_{ij}} (\Phi^i_{o_{j,r}})_l^{(n+1)} \phi^i_{j,r}(\mathbf{x}), \quad \mathbf{x} \in e_{ij}\end{aligned} \tag{14}$$

where l refers to the iteration number of Newton–Raphson's iterations, $\phi^i_{j,r}(\mathbf{x})$ are the shape functions, $r = 0, 1, \ldots, R_{i,j}$, $R_{ij}+1$ is the total number of interpolation points for $(\Phi_{\alpha h})_l^{(n+1)}$ on e_{ij}, and $(\Phi^i_{\alpha_{j,r}})_l^{(n+1)}$ denotes the nodal value of $(\Phi_{\alpha h})_l^{(n+1)}$, $\alpha = \mathrm{w}, \mathrm{o}$. Since δp, δp_b, and δs_w at grid points in all time steps need to be obtained for this state, we approximate the lth iteration values of these variables at the $(n+1)$th time step by

$$\begin{aligned}(\delta p_h)_l^{(n+1)} &= \sum_{r=0}^{R_{ij}} (\delta p^i_{j,r})_l^{(n+1)} \phi^i_{j,r}(\mathbf{x}), \quad \mathbf{x} \in e_{ij} \\ (\delta s_{wh})_l^{(n+1)} &= \sum_{r=0}^{R_{ij}} (\delta s^i_{w_{j,r}})_l^{(n+1)} \phi^i_{j,r}(\mathbf{x}), \quad \mathbf{x} \in e_{ij} \\ (\delta p_{bh})_l^{(n+1)} &= \sum_{r=0}^{R_{ij}} (\delta p^i_{b_{j,r}})_l^{(n+1)} \phi^i_{j,r}(\mathbf{x}), \quad \mathbf{x} \in e_{ij}\end{aligned} \tag{15}$$

We substitute these interpolants into the linearized governing equations to obtain the discrete equations. In these discrete equations, the lth iteration values of increments $(\delta p^i_{j,r})_l^{(n+1)}$, $(\delta s^i_{w_{j,r}})_l^{(n+1)}$, and $(\delta p^i_{b_{j,r}})_l^{(n+1)}$ at the $(n+1)$th time step at nodes $\mathbf{x}^i_{j,r}$ are the unknowns to be solved for. For a well with a flow rate control, the increment of its bottom hole pressure p_{bh} also needs to be obtained. After these increments are obtained, the iteration solutions at grid point $\mathbf{x}_i$ and the bottom hole pressure of the kth well are updated by

$$\begin{aligned}(p_i)_{l+1}^{(n+1)} &= (p_i)_l^{(n+1)} + (\delta p_i)_l^{(n+1)} \\ (s_{wi})_{l+1}^{(n+1)} &= (s_{wi})_l^{(n+1)} + (\delta s_{wi})_l^{(n+1)} \\ (p_{bi})_{l+1}^{(n+1)} &= (p_{bi})_l^{(n+1)} + (\delta p_{bi})_l^{(n+1)} \\ (p_{bh,k})_{l+1}^{(n+1)} &= (p_{bh,k})_l^{(n+1)} + (\delta p_{bh,k})_l^{(n+1)}\end{aligned} \tag{16}$$

Similarly, in the saturated state, we approximate the lth iteration values of the water, oil, and gas potentials at the $(n+1)$th time step by

$$\begin{aligned}(\Phi_{wh})_l^{(n+1)} &= \sum_{r=0}^{R_{ij}} (\Phi^i_{w_{j,r}})_l^{(n+1)} \phi^i_{j,r}(\mathbf{x}), \quad \mathbf{x} \in e_{ij} \\ (\Phi_{oh})_l^{(n+1)} &= \sum_{r=0}^{R_{ij}} (\Phi^i_{o_{j,r}})_l^{(n+1)} \phi^i_{j,r}(\mathbf{x}), \quad \mathbf{x} \in e_{ij} \\ (\Phi_{gh})_l^{(n+1)} &= \sum_{r=0}^{R_{ij}} (\Phi^i_{g_{j,r}})_l^{(n+1)} \phi^i_{j,r}(\mathbf{x}), \quad \mathbf{x} \in e_{ij}\end{aligned} \tag{17}$$

and approximate the unknowns $(\delta p)_l^{(n+1)}$, $(\delta s_{\mathrm{w}})_l^{(n+1)}$, and $(\delta s_{\mathrm{o}})_l^{(n+1)}$ by

$$\begin{aligned}
(\delta p_h)_l^{(n+1)} &= \sum_{r=0}^{R_{ij}} (\delta p_{j,r}^i)_l^{(n+1)} \phi_{j,r}^i(\mathbf{x}), \quad \mathbf{x} \in e_{ij} \\
(\delta s_{\mathrm{w}h})_l^{(n+1)} &= \sum_{r=0}^{R_{ij}} (\delta s_{\mathrm{w}_{j,r}}^i)_l^{(n+1)} \phi_{j,r}^i(\mathbf{x}), \quad \mathbf{x} \in e_{ij} \\
(\delta s_{\mathrm{o}h})_l^{(n+1)} &= \sum_{r=0}^{R_{ij}} (\delta s_{\mathrm{o}_{j,r}}^i)_l^{(n+1)} \phi_{j,r}^i(\mathbf{x}), \quad \mathbf{x} \in e_{ij}
\end{aligned} \tag{18}$$

We substitute them into the linearized governing equations to get the discrete equations. The iteration solution values at grid point $\mathbf{x}_i$ and the kth well, which has a flow rate control, are updated by

$$\begin{aligned}
(p_i)_{l+1}^{(n+1)} &= (p_i)_l^{(n+1)} + (\delta p_i)_l^{(n+1)} \\
(s_{\mathrm{w}i})_{l+1}^{(n+1)} &= (s_{\mathrm{w}i})_l^{(n+1)} + (\delta s_{\mathrm{w}i})_l^{(n+1)} \\
(s_{\mathrm{o}i})_{l+1}^{(n+1)} &= (s_{\mathrm{o}i})_l^{(n+1)} + (\delta s_{\mathrm{o}i})_l^{(n+1)} \\
(p_{\mathrm{b}h,k})_{l+1}^{(n+1)} &= (p_{\mathrm{b}h,k})_l^{(n+1)} + (\delta p_{\mathrm{b}h,k})_l^{(n+1)}
\end{aligned} \tag{19}$$

We remark that different states at different places in a reservoir can occur; i.e. the saturated and undersaturated states can co-exist. In this case, the governing equations on each control volume are linearized and discretized according to the state in this volume.

The form of the coefficient matrix of the system arising from the discretization of the black oil model using the CVFA depends on the type of control volumes used. An example of hybrid grids in reservoir simulation is shown in Figure 1, where a cross section in the horizontal direction is illustrated. The base grid in this direction consists of hexagons; the grid near a vertical well is circular, and it is rectangular near a slanted well. The hexagons can effectively reduce grid orientation effects [6]. For a reservoir that has a layer structure,

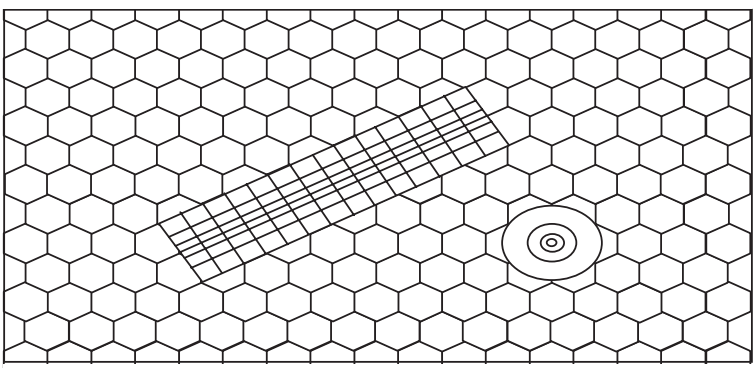

Figure 1. Grid modules.

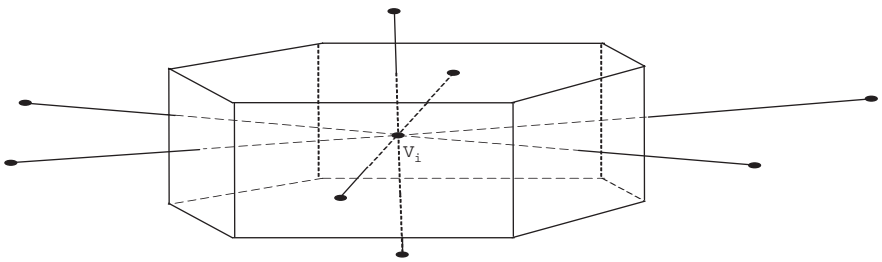

Figure 2. Control volume V_i.

hexagonal prisms (hexagons in the horizontal direction and rectangles in the vertical direction) can be utilized; see Figure 2. For this type of grids, the system of algebraic equations is of the form

$$\begin{pmatrix} A_{gg} & A_{gw} \\ A_{wg} & A_{ww} \end{pmatrix} \begin{pmatrix} X_g \\ X_w \end{pmatrix} = \begin{pmatrix} \mathrm{RHS}_g \\ \mathrm{RHS}_w \end{pmatrix} \tag{20}$$

where X_g and X_w are the unknown vector at grid nodes and the bottom hole pressure unknown vector at wells, A_{gg} and A_{ww} are the sub-matrices associated with the grid nodes and wells, respectively, and A_{gw} and A_{wg} are the interaction sub-matrices between the grid nodes and wells. As noted, this system is non-symmetric. Moreover, the band structure of the coefficient matrix in (20) is spoiled by wells that perforate into many gridblocks and by irregular grid structure. In this paper we investigate the application of ORTHOMIN and GMRES to (20), and numerically carry out comparisons between these two solvers.

3. ORTHOMIN AND GMRES

ORTHOMIN is a truncated version of the generalized conjugate residual (GCR) algorithm and an efficient iterative solver for petroleum reservoir simulation [8]. For the purpose of comparison, a general ORTHOMIN(K) is briefly reviewed in Algorithm 1 for solution of a left-preconditioned system

$$M^{-1}Ax = M^{-1}b$$

In Algorithm 1, for the purpose of illustration, $M = LU$ is an ILU factorization of A. A left-preconditioned GMRES is described in Algorithm 2, where $\hat{H}_m$ is the upper Hessenberg from the Gram–Schmidt process. A variant of GMRES, flexible GMRES (FGMRES) [15], uses a different preconditioner at each step of the Arnoldi process. The Arnoldi process simply constructs an orthogonal basis for the preconditioned Krylov subspace

$$\kappa_m = \mathrm{span}\{r_0, M_1^{-1}Ar_0, \ldots, (M_1^{-1}A)\cdots(M_{m-1}^{-1}A)r_0\}$$

The difference between GMRES and FGMRES is that for GMRES, all the $M_i = M$ are the same, and $z_i = M^{-1}v_i$ need not be stored for right preconditioners during computations.

Algorithm 1.

ORTHOMIN(K)

1. $M = LU$, where LU is an ILU factorization of A
2. **Start:** Set $r = b$, $x = p_0 = 0$, $Iter = 0$, and the values of $\varepsilon, \mathrm{ITMAX}, K$
3. **Iteration:**
   (a) For $k = 1, K$ do
      i. $Iter = Iter + 1$
      ii. $u_k = M^{-1} r_{k-1}$
      iii. $v_k = A u_k$
      iv. $p_k = u_k$
      v. $q_k = v_k$
      vi. For $1 \leqslant j < k$, *do* $\begin{cases} \alpha_{jk} = (q_j, v_k)/(q_j, q_j) \\ p_k = p_k - \alpha_{jk} p_j \\ q_k = q_k - \alpha_{jk} q_j \end{cases}$
      vii. $\beta_k = (q_k, r_{k-1})/(q_k, q_k)$
      viii. $x_k = x_{k-1} + \beta_k p_k$
      ix. $r_k = r_{k-1} - \beta_k q_k$
      x. Compute $\|r_k\|_2$, $RMX = \|r_k\|_2/\|b\|_2$
      xi. If ($RMX \leqslant \varepsilon$ or $Iter \geqslant \mathrm{ITMAX}$), go to 4.
   (b) End do
   (c) $r_0 = r_K$
   (d) $x_0 = x_K$
   (e) Go to (a)
4. **End iteration**

Algorithm 2.

Left preconditioned GMRES(m)

1. $M = LU$, where LU is an ILU factorization of A
2. **Start:** Choose an initial guess x_0 and the dimension of the Krylov subspace m. Set up a $(m+1) \times m$ matrix $\hat{H}_m$ with zero entries.
3. **Arnoldi process:**
   (a) Compute $r_0 = M^{-1}(b - Ax_0)$, $\beta = \|r_0\|_2$, and $v_1 = r_0/\beta$
   (b) For $j = 1, \ldots, m$, do
      - Compute $w_j = M^{-1} A v_j$
      - For $i = 1, \ldots, j$, $\begin{cases} h_{ij} = (w_j, v_i) \\ w_j = w_j - h_{ij} v_i \end{cases}$
      - Compute $h_{j+1,j} = \|w_j\|_2$ and $v_{j+1} = w_j/\|w_j\|_2$
   (c) Define $Z_m = [v_1, \ldots, v_m]$.
4. **Update:** $x_m = x_0 + Z_m y_m$, where

$$y_m = \mathrm{argmin} \|\beta e_1 - \hat{H}_m y\|_2$$

5. **Restart:** If convergent, stop; else, $x_0 = x_m$ and go to 3

FGMRES is more flexible and suitable to solution of difficult problems with complex preconditioners.

4. COMPARISONS

We assume that the same preconditioner M is used for both algorithms. Let STP and STA be the amount of storage for M and A, and let FLOPP and FLOPA be the total flops of computing $M^{-1}x$ and Ax, respectively, where x is a vector. Below we compare ORTHOMIN and GMRES in terms of the storage and total flops per restart. The definition of a flop follows Moler [16]; i.e. a flop involves the operation $s + a * b$.

4.1. Comparison in terms of storage

Let NEQ be the number of partial differential equations (e.g. NEQ = 3 for the black oil model), NCV be the number of grids in the simulation domain, and NRSTRT be the number of restarts, i.e. the number of vectors in the Krylov subspace.

For ORTHOMIN, its main storage is as follows:

- Coefficient matrix: STA
- Preconditioner matrix: STP
- Krylov vector space: $2 * \text{NEQ} * \text{NCV} * \text{NRSTRT}$
- Other vectors such as RHS, RES, RA, RR: $4 * \text{NEQ} * \text{NCV}$
- Total storage: $\text{STA} + \text{STP} + 2 * \text{NEQ} * \text{NCV} * \text{NRSTRT} + 4 * \text{NEQ} * \text{NCV}$

For GMRES, its main storage is given below:

- Coefficient matrix: STA
- Preconditioner matrix: STP
- Krylov vector space: $\text{NEQ} * \text{NCV} * \text{NRSTRT}$
- Vector space $Z_{\text{NRSTRT}} = [z_1, \ldots, z_{\text{NRSTRT}}]$: $\text{NEQ} * \text{NCV} * \text{NRSTRT}$
- Other vectors such as RHS, RES: $2\text{NEQ} * \text{NCV}$
- Matrix $\hat{H}_m$: $(\text{NRSTRT} + 1) * (\text{NRSTRT} + 6) + 3 * \text{NRSTRT} + 2$
- Total storage: $\text{STA}+\text{STP}+2 * \text{NEQ} * \text{NCV} * \text{NRSTRT}+2 * \text{NEQ} * \text{NCV}+(\text{NRSTRT}+1) * (\text{NRSTRT} + 6) + 3 * \text{NRSTRT} + 2$

From these two counts, we see that when $\text{NCV} * \text{NEQ} > (\text{NRSTRT} + 5)^2/2$, the amount of storage of ORTHOMIN is bigger than that of GMRES.

4.2. Comparison in terms of total flops

For convenience, we consider the total flops of both algorithms per restart step.

For ORTHOMIN, its main computational flops are

- Coefficient matrix: $\text{FLOPA} * \text{NRSTRT}$
- Preconditioner matrix: $\text{FLOPP} * \text{NRSTRT}$
- Inner product: $\{\text{NRSTRT}/2 + 2 * (\text{NRSTRT} + 1) * \text{NRSTRT}/2 + 2 * \text{NRSTRT}\} * (\text{NEQ} * \text{NCV}/2) = (\text{NRSTRT}/2 + 7/4) * \text{NEQ} * \text{NCV} * \text{NRSTRT}$
- Vector update: $\{4 + (\text{NRSTRT} + 1)\} * \text{NEQ} * \text{NCV} * \text{NRSTRT} = (\text{NRSTRT} + 5) * \text{NEQ} * \text{NCV} * \text{NRSTRT}$

- Total flop count: $\{\text{FLOPA}+\text{FLOPP}+((\text{NRSTRT}/2+7/4)+4+(\text{NRSTRT}+1))*\text{NEQ}*\text{NCV}\}*\text{NRSTRT}=\{\text{FLOPA}+\text{FLOPP}+(\text{NRSTRT}*3/2+27/4)*\text{NEQ}*\text{NCV}\}*\text{NRSTRT}$

For GMRES, its main computational flops are

- Coefficient matrix: $\text{FLOPA}*\text{NRSTRT}$
- Preconditioner matrix: $\text{FLOPP}*\text{NRSTRT}$
- Inner product: $\{(\text{NRSTRT}+1)*\text{NRSTRT}/2+\text{NRSTRT}\}*(\text{NEQ}*\text{NCV}/2)=(\text{NRSTRT}/4+3/4)*\text{NEQ}*\text{NCV}*\text{NRSTRT}$
- Vector update: $\{(\text{NRSTRT}+1)/2+1+1\}*\text{NEQ}*\text{NCV}*\text{NRSTRT}=(\text{NRSTRT}/2+5/2)*\text{NEQ}*\text{NCV}*\text{NRSTRT}$
- Solving $y_m=\text{argmin}\|\beta e_1-\hat{H}_m y\|_2$: $(\text{NRSTRT}+1)*\text{NRSTRT}/2$
- Total flop count: $\{\text{FLOPA}+\text{FLOPP}+((\text{NRSTRT}/4+3/4)+(\text{NRSTRT}/2+5/2))*\text{NEQ}*\text{NCV}\}*\text{NRSTRT}+(\text{NRSTRT}+1)*\text{NRSTRT}/2=\{\text{FLOPA}+\text{FLOPP}+(\text{NRSTRT}*3/4+13/4)*\text{NEQ}*\text{NCV}\}*\text{NRSTRT}+(\text{NRSTRT}+1)*\text{NRSTRT}/2$

From these total flop counts, we see that when $\text{NCV}>\text{NRSTRT}$, in each restart step the total flops of ORTHOMIN are bigger than those of GMRES.

Our simulator SMU02 is a general multicomponent, multiphase reservoir simulator based on the black oil model. It includes rectangular, PEBI, and Voronoi gridding techniques and finite difference, control volume finite element, and control volume function approximation discretization methods [17]. It consists of two major parts: the initialization SMU02I and the main body SMU02R. In the SMU02I, data such as fluid, rock, injection, production, grid, and control data are read from initial files, and then necessary data preparations are done for the SMU02R.

The SMU02R includes some major components like time and space discretization of the governing equations, Newton–Raphson linearizations, construction of Jacobian matrices, solution of linear systems, and visualization of outputs. The solution of linear systems is within each Newton–Raphson iteration. As mentioned, for a petroleum reservoir simulation with a number of gridblocks of order 100 000, about 80–90% of the total simulation time is spent on the system solution. The linear solvers in SMU02R are based on ORTHOMIN(K) and GMRES(m), with the preconditioners ILU(K) and ILUT(K) (a dual threshold incomplete LU factorization). In the comparison of these two solvers, we use ILU(K) as the preconditioners for both of them.

5. NUMERICAL EXPERIMENTS

We carry out numerical experiments on a shared-memory machine, SGI Origin 2000 with 8 250 MHz processors and 4 G memory; each processor has 32 KB L1 cache for instructions, 32 KB L1 cache for data, and 4 MB L2 cache [18]. The convergent criterion for both ORTHOMIN and GMRES is $\|r_k\|_2/\|\text{RHS}\|_2\leqslant 10^{-4}$. As noted, the solution scheme is based on the fully implicit solution method; i.e. all the coupled equations are solved simultaneously and implicitly. The number of restarts is ten, and the ILU(0) is used as the preconditioner for both ORTHOMIN and GMRES.

In the subsequent tables TT and ST indicate the total and solver CPU times in seconds, respectively. NX, NY, and NZ are the number of grid blocks in the x-, y- and z-axis, DELTX and DELTY are the length of the blocks in the x- and y-axis, respectively, and NWELL is the number of wells simulated.

5.1. A SPE problem

5.1.1. SPE1. This simulation problem is chosen from the second case of the benchmark problem of the first CSP [19]. A grid of rectangular parallelepipeds for the reservoir under consideration is given in Figure 3, where the number of subintervals in the x-, y- and z-direction is 10, 10, and 3, respectively. The diagonal cross-sectional view of this reservoir can be also seen in this figure. We briefly state the data; for more details on these data, see Reference [19]. While a rectangular grid is shown in Figure 3, hexagonal prisms displayed in Figure 2 are employed in the CVFA.

At the initial state, the reservoir reaches equilibrium with initial reservoir pressure 4800 psia at 8400 ft and with reservoir temperature 200°F. The depth to the top of this reservoir is 8325 ft. The gas–oil (GOC) and water–oil contacts (WOC) are, respectively, located at 8320 and 8450 ft. The capillary pressure is zero. The reservoir porosity measured at a pressure of 14.7 psia is 0.3. The rock compressibility is 3×10^{-6} 1/psi. The PVT function data for oil, water, and gas are, respectively, given in Tables I–V, where FVF stands for the formation

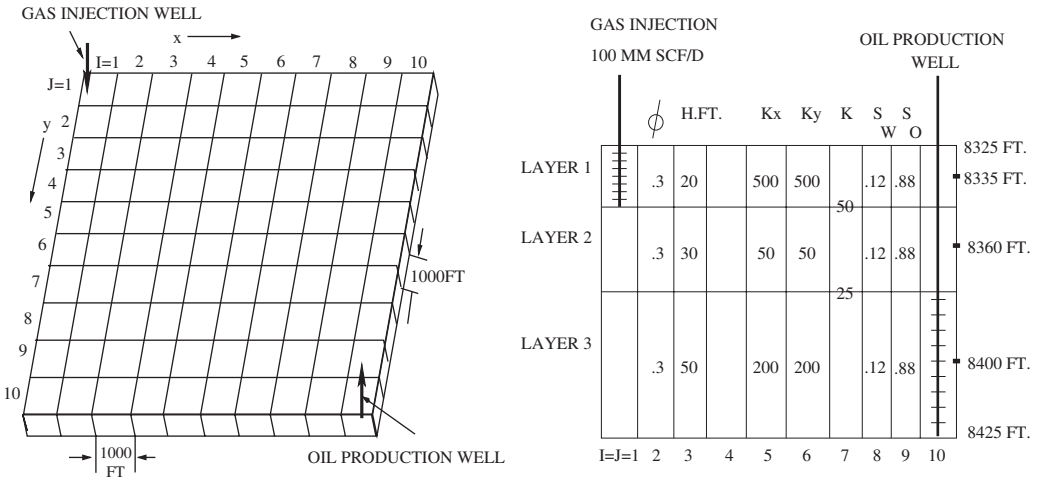

Figure 3. Left: reservoir; right: diagonal cross section.

Table I. Saturated oil PVT function data.

Pressure (psia)	FVF (RB/STB)	Viscosity (cp)	Density (lb m/ft^3)	Solution GOR (SCF/STB)
14.7	1.0620	1.0400	46.244	1.0
264.7	1.1500	0.9750	43.544	90.5
514.7	1.2070	0.9100	42.287	180.0
1014.7	1.2950	0.8300	41.004	371.0
2014.7	1.4350	0.6950	38.995	636.0
2514.7	1.5000	0.6410	38.304	775.0
3014.7	1.5650	0.5940	37.781	930.0
4014.7	1.6950	0.5100	37.046	1270.0
5014.7	1.8270	0.4490	36.424	1618.0
9014.7	2.3570	0.2030	36.482	2984.0

Table II. Saturated water PVT function data.

Pressure (psia)	FVF (RB/STB)	Viscosity (cp)	Density ($lb\,m/ft^3$)	Gas/water ratio (SCF/STB)
14.7	1.0410	0.3100	62.238	0.0
264.7	1.0403	0.3100	62.283	0.0
514.7	1.0395	0.3100	62.328	0.0
1014.7	1.0380	0.3100	62.418	0.0
2014.7	1.0350	0.3100	62.599	0.0
2514.7	1.0335	0.3100	62.690	0.0
3014.7	1.0320	0.3100	62.781	0.0
4014.7	1.0290	0.3100	62.964	0.0
5014.7	1.0258	0.3100	63.160	0.0
9014.7	1.0130	0.3100	63.959	0.0

Table III. Gas PVT function data.

Pressure (psia)	FVF (RB/STB)	Viscosity (cp)	Density ($lb\,m/ft^3$)	Pseudo gas potential (psia/cp)
14.7	0.166666	0.008000	0.0647	0
264.7	0.012093	0.009600	0.8916	0.777916 E+07
514.7	0.006274	0.011200	1.7185	0.267580 E+08
1014.7	0.003197	0.014000	3.3727	0.875262 E+08
2014.7	0.001614	0.018900	6.6806	0.270709 E+09
2514.7	0.001294	0.020800	8.3326	0.386910 E+09
3014.7	0.001080	0.022800	9.9837	0.516118 E+09
4014.7	0.000811	0.026800	13.2952	0.803963 E+09
5014.7	0.000649	0.030900	16.6139	0.112256 E+10
9014.7	0.000386	0.047000	27.9483	0.251845 E+10

Table IV. Undersaturated oil PVT function data.

Pressure (psia)	FVF (RB/STB)	Viscosity (cp)	Density ($lb\,m/ft^3$)
4014.7	1.6950	0.5100	37.046
9014.7	1.5790	0.7400	39.768

Table V. Undersaturated water PVT function data.

Pressure (psia)	FVF (RB/STB)	Viscosity (cp)	Density ($lb\,m/ft^3$)
4014.7	1.0290	0.3100	62.964
9014.7	1.0130	0.3100	63.959

Table VI. Relative permeability data of model I.

s_g	K_{rg}	K_{ro}
0.0	0.0	1.0
0.001	0.0	1.0
0.02	0.0	0.997
0.05	0.005	0.980
0.12	0.025	0.700
0.2	0.075	0.350
0.25	0.125	0.200
0.30	0.190	0.090
0.40	0.410	0.021
0.45	0.60	0.010
0.50	0.72	0.001
0.60	0.87	0.0001
0.70	0.94	0.000
0.85	0.98	0.000
1.0	1.0	0.000

Table VII. Partition information for the SPE model.

NX	NY	NZ	NWELL	DELTX	DELTY
10	10	3	2	1000	1000

Table VIII. CPU times and flops of ORTHOMIN and GMRES for the SPE model.

Method	TT (s)	ST (s)	Flops per iteration	Days
ORTHOMIN	204.91	174.08	519 750	3650.0
GMRES	172.06	141.22	420 805	3650.0

volume factor. The horizontal and vertical absolute permeability distribution and the initial water and oil saturation distribution are indicated in Figure 3. The saturation function data are listed in Table VI.

There are a gas injection well and an oil production well (Table VII), whose wellbore radii are 0.25 ft. Their locations are shown in Figure 3. They completely perforate at the first and third zone, respectively. The gas injection rate is 100 MMSCF/D. The maximum and minimum oil production rates of the production well are, respectively, 20 000 STB/D and 1000 STB/D, and the minimum flowing bottom hole pressure is 1000 psia. The run of the simulator is terminated at the end of the 10th year. The CPU times for ORTHOMIN and GMRES and their flops per iteration are displayed in Table VIII. From this table we do see speed-up of GMRES for this simulation problem; GMRES uses 81.12% of ORTHOMIN's CPU time. The average reservoir pressure, gas–oil ratio, oil production rate, and oil recovery curves obtained by these two algorithms are shown in Figures 4 and 5. These curves match well for the two different algorithms.

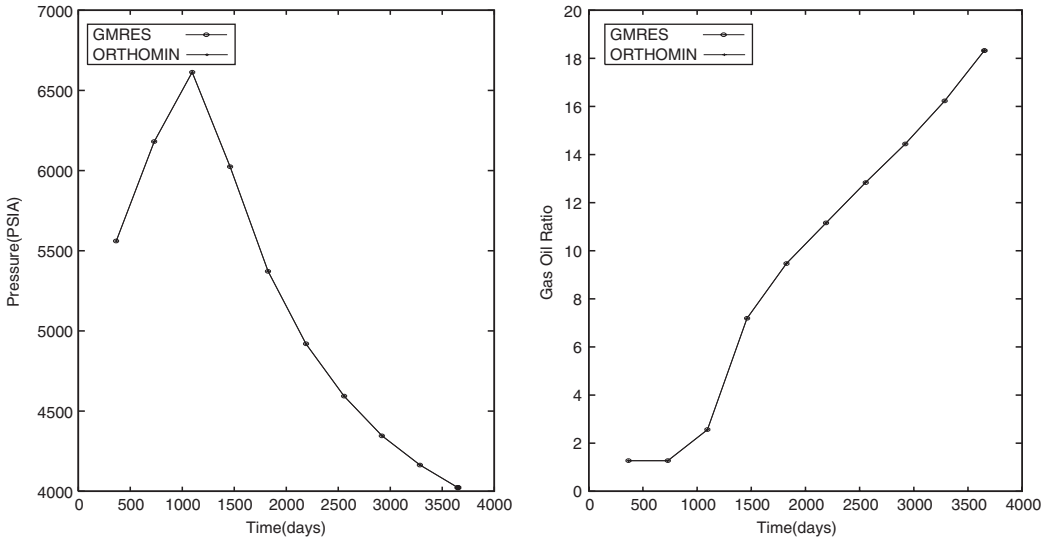

Figure 4. Left: pressure curve; right: gas–oil ratio curve.

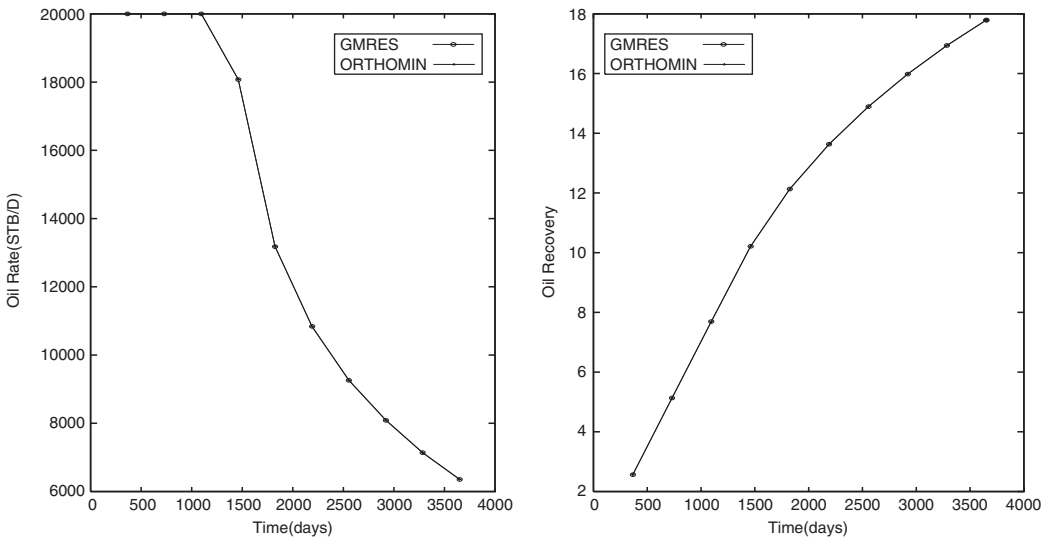

Figure 5. Left: oil production rate curve; right: oil recovery curve.

5.1.2. SPE1: refined. This model problem is the same as the previous one. We just refine the grid in the x- and y-directions. Now, the number of subintervals in these two directions is 70, and the total number of grid points is 14 700. For such a simulation problem with small grid blocks and with a long simulation time (10 years), stability of the numerical solution to the problem is very important. Both ORTHOMIN and GMRES work very well for this problem;

Table IX. CPU times and flops of ORTHOMIN and GMRES for the refined SPE model.

Method	TT (s)	ST (s)	Flops per iteration	Days
ORTHOMIN	70 480.36	63 798.47	25 467 750	3650.0
GMRES	45 605.43	39 071.48	20 616 805	3650.0

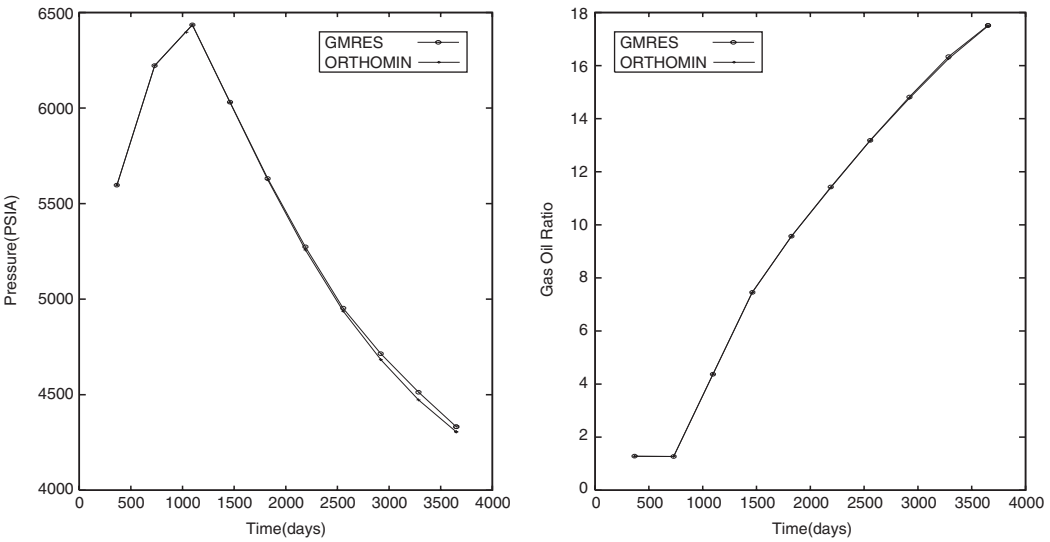

Figure 6. Left: pressure curve; right: gas–oil ratio curve.

their CPU times and flops per iteration are given in Table IX. We see that GMRES uses only 61.24% of the CPU time of ORTHOMIN when the grid is refined. The average pressure, gas–oil ratio, oil production rate, and oil recovery curves obtained by these two algorithms are shown in Figures 6 and 7. Again, these curves match well for the two different algorithms.

5.1.3. SPE1: relationship between the numbers of unknowns and iterations. To see how the numbers of linear (the linear solvers) and nonlinear (the Newton–Raphson iterations) iterations depend on the number of unknowns, we consider the following refinements for the SPE1 case 2:

1. $\mathrm{NX} = 10$, $\mathrm{NY} = 10$, and $\mathrm{NZ} = 3$ (the original SPE1 case 2),
2. $\mathrm{NX} = 30$, $\mathrm{NY} = 30$, and $\mathrm{NZ} = 3$,
3. $\mathrm{NX} = 50$, $\mathrm{NY} = 50$, and $\mathrm{NZ} = 3$,
4. $\mathrm{NX} = 70$, $\mathrm{NY} = 70$, and $\mathrm{NZ} = 3$.

All simulation experiments were conducted with a final time of 3650 days. The simulation results are given in Tables X and XI and Figures 8 and 9.It follows from these tables and figures that the numbers of linear and nonlinear iterations for both GMRES and ORTHOMIN increase nonlinearly with the number of unknowns, the linear iteration numbers are better for

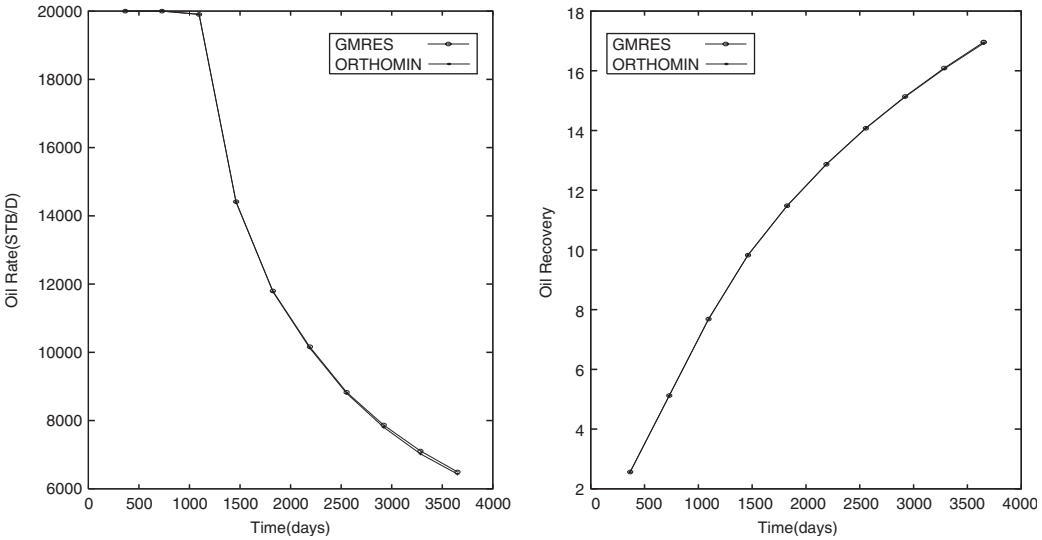

Figure 7. Left: oil production rate curve; right: oil recovery curve.

Table X. Comparison of the dependence of the number of linear iterations on the number of unknowns.

Problems	Number of unknowns	Linear iters of GMRES	Linear iters of ORTHOMIN	GMRES: Flops per iteration	ORTHOMIN: Flops per iteration
$10 \times 10 \times 3$	300	13 280	13 303	420 805	519 750
$30 \times 30 \times 3$	2700	42 136	54 174	3 786 805	4 677 750
$50 \times 50 \times 3$	7500	67 441	99 473	10 518 805	12 993 750
$70 \times 70 \times 3$	14 700	97 749	155 039	20 616 805	25 467 750

Table XI. Comparison of the dependence of the number of nonlinear iterations on the number of unknowns.

Problems	Number of unknowns	Nonlinear iters of GMRES	Nonlinear iters of ORTHOMIN
$10 \times 10 \times 3$	300	475	476
$30 \times 30 \times 3$	2700	1081	1081
$50 \times 50 \times 3$	7500	1652	1635
$70 \times 70 \times 3$	14 700	2167	2183

GMRES than for ORTHOMIN, particularly for problems of larger sizes, and the nonlinear iteration numbers are almost the same for both algorithms.

5.2. A real oil field problem

We now compare ORTHOMIN and GMRES for a large, real oil reservoir in South America to simulate the behaviour of a water flooding process and to predict the performance of this

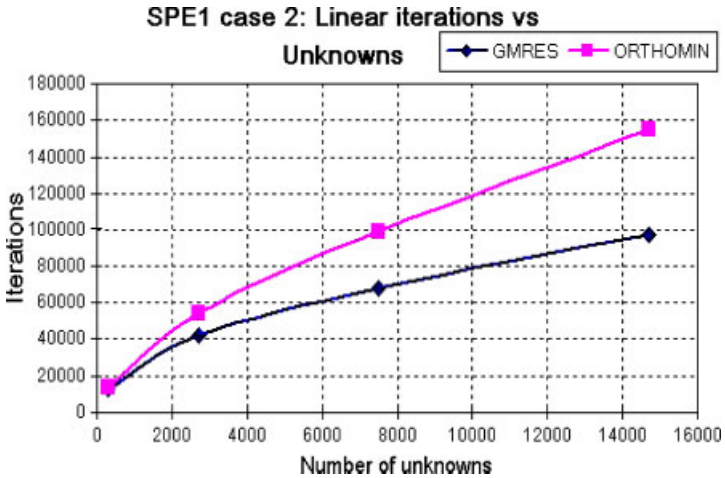

Figure 8. Dependence of the number of linear iterations on the number of unknowns.

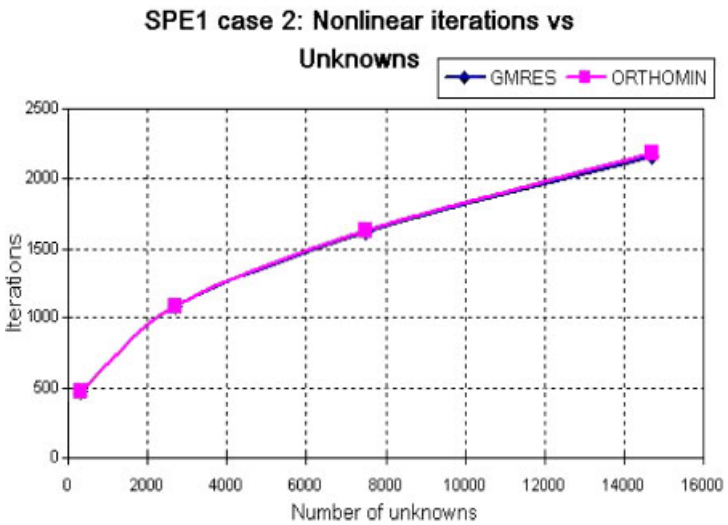

Figure 9. Dependence of the number of nonlinear iterations on the number of unknowns.

reservoir. The outline of this reservoir is as follows:

- The initial formation pressure equals 11 800 psia and the initial bubble point pressure is 3157 psia.
- The datum depth is 15 500 ft and the depth of WOC is 17 200 ft.
- The surface oil density is 57.06 lbm ft^3, the oil formation factor is 1.446, the oil viscosity in the reservoir is 0.679 cp, and the oil–water viscosity ratio is 3.3.

Table XII. Partition information for the real oil field model.

NX	NY	NZ	NWELL	DELTX	DELTY
64	31	40	24	410	410

Table XIII. CPU times and flops of ORTHOMIN and GMRES for the real oil field model.

Method	TT (s)	ST (s)	Flops per iteration	Days
ORTHOMIN	68 518.80	60 923.75	91 660 800	4901.0
GMRES	50 497.55	42 889.26	74 201 655	4901.0

- The geological features are: 40 sandstone layers; the 11th and 30th layers—sealing; three independent development units divided in the vertical direction; the western and eastern regions divided by a fault in the reservoir.
- The reservoir has been developed for 13.5 years: 5.3 years—natural reservoir drive; 8.2 years—water injection.
- 24 wells have been drilled. Ten oil production wells and 5 water injection wells are used to develop this reservoir in the current period.

5.2.1. 3D two-phase flow problem. The first case is a two-phase (water and oil) flow problem in three dimensions. The dimensions of the partition of the simulation domain Ω is given in Table XII. The CPU times and flops per iteration for ORTHOMIN and GMRES are displayed in Table XIII. From this table we again see speed-up of GMRES for this flow problem; GMRES uses 70.4% of ORTHOMIN's CPU time. The average pressure, water cut, daily oil production rate, and oil recovery curves obtained by these two algorithms are shown in Figures 10 and 11.These curves match well.

5.2.2. 3D three-phase flow problem. The second case simulates a three-phase (water, oil, and gas) flow problem, with the same partition as in Table XII. The numerical results are displayed in Table XIV and Figures 12 and 13. Now, GMRES uses only 66.41% of the CPU time of ORTHOMIN for this three-phase flow problem.

5.2.3. 3D three-phase problem with a horizontal well. The third case is the same as the second case considered above, except that a horizontal production well is added now. The numerical results are stated in Table XV and Figures 14 and 15. Now, we see that the GMRES uses only 69.54% of the CPU time of ORTHOMIN for this three-phase flow problem.

5.3. Concluding remarks

In this paper we have discussed and implemented ORTHOMIN and GMRES for solution of linear systems arising from the discretization of the black oil model using the CVFA on unstructured grids. Numerical comparisons between these two algorithms have been presented for a SPE problem and a real oil field problem. Based on the numerical results, we can draw

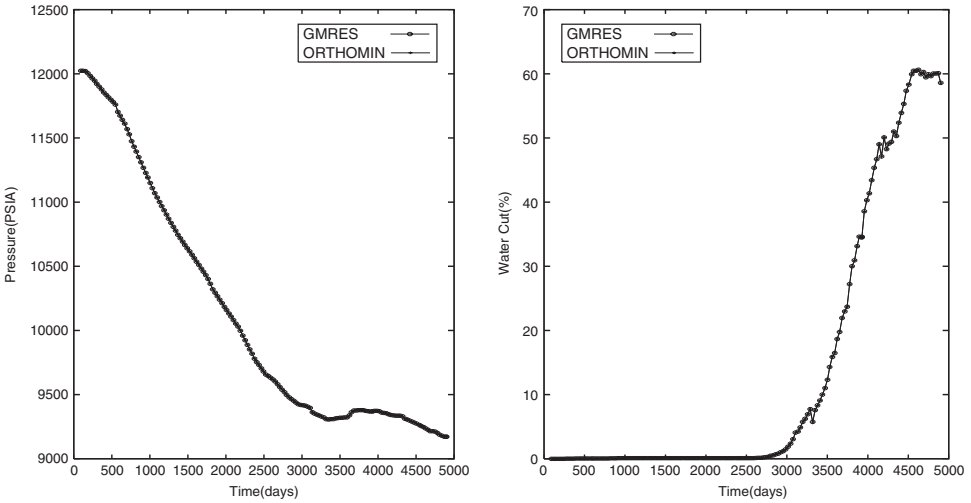

Figure 10. Left: pressure curve; right: water cut curve.

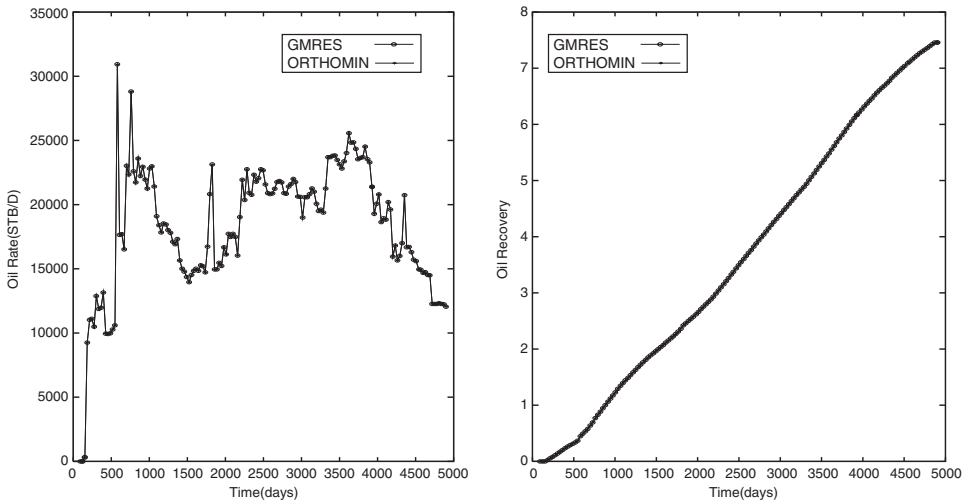

Figure 11. Left: daily oil production rate; right: oil recovery curve.

Table XIV. CPU times and flops of ORTHOMIN and GMRES for three phases.

Method	TT (s)	ST (s)	Flops per iteration	Days
ORTHOMIN	199 403.32	178 974.25	137 491 200	4901.0
GMRES	141 168.79	118 853.82	111 302 455	4901.0

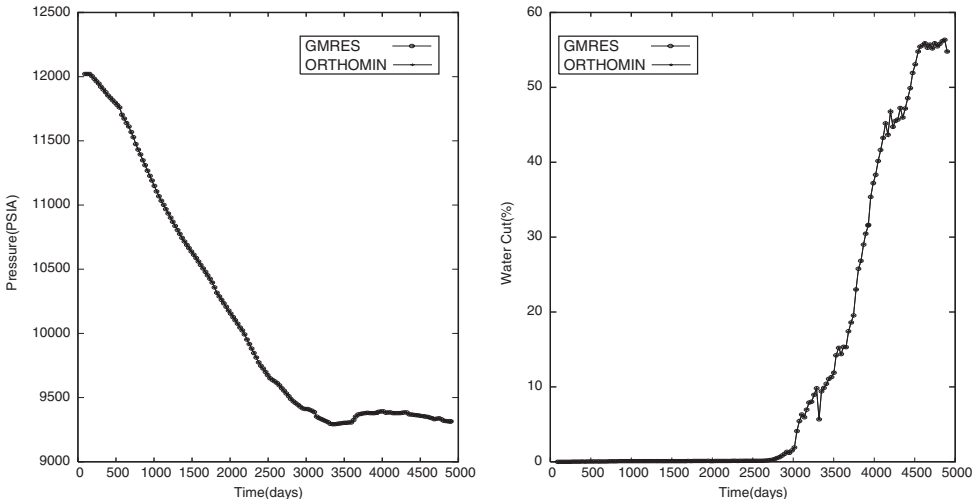

Figure 12. Left: pressure curve; right: water cut curve.

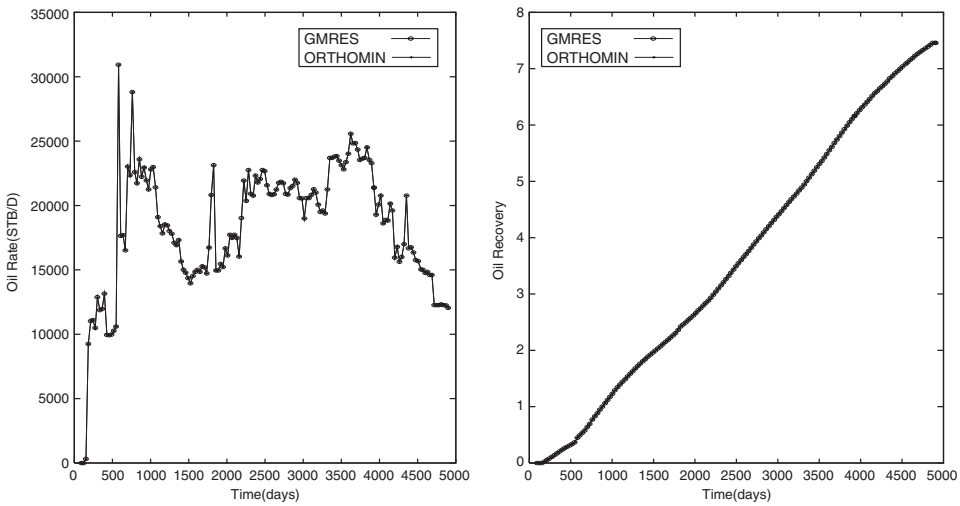

Figure 13. Left: daily oil production rate; right: oil recovery curve.

Table XV. CPU times of ORTHOMIN and GMRES with a horizontal well.

Method	TT (s)	ST (s)	Days
ORTHOMIN	468 184.48	438 123.19	6726.0
GMRES	345 927.49	304 688.44	6726.0

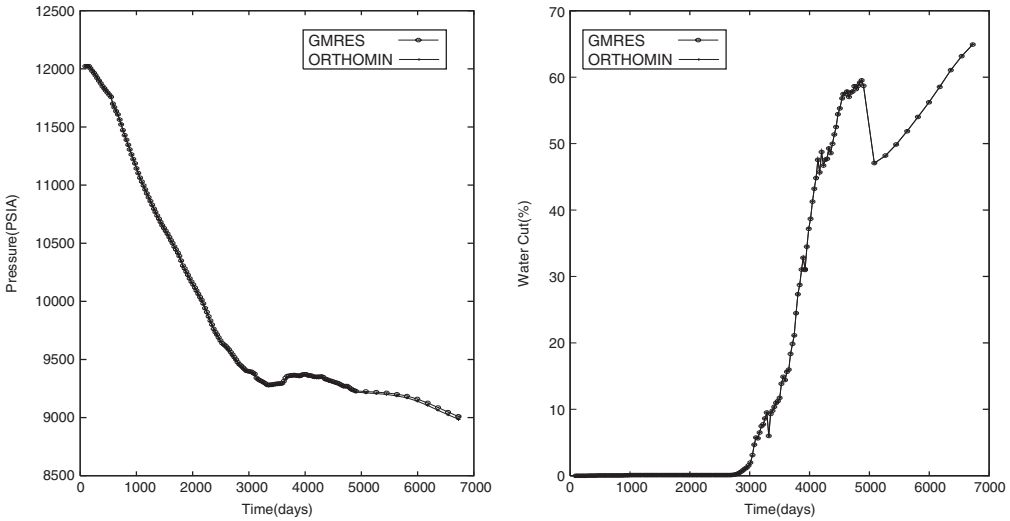

Figure 14. Left: pressure curve; right: water cut curve.

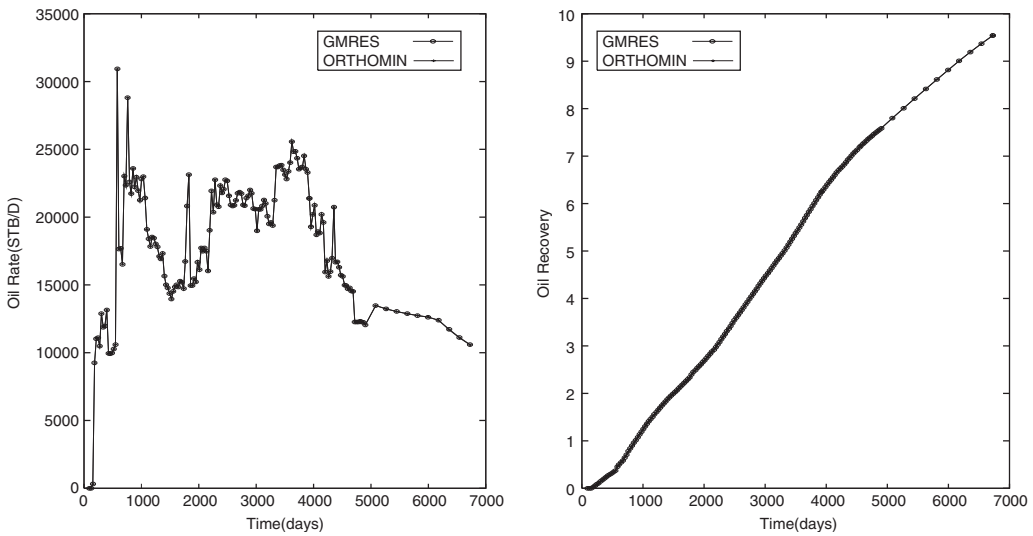

Figure 15. Left: daily oil production rate; right: oil recovery curve.

the following conclusions:

- ORTHOMIN and GMRES have the same stability for all the tested problems in terms of reservoir properties such as the average pressure, gas–oil ratio, oil production rate, oil recovery, and water cut.
- GMRES is faster than ORTHOMIN for all the tested problems in terms of the total and solver CPU times. The more efficiency of GMRES can be particularly seen for large-scale complex multiphase flow problems.

- As the scale of tested problems increases, GMRES's efficiency increases, as the SPE problem and its refinement have shown. As the complexity of tested problems increases, GMRES's efficiency increases as well, as the real oil field problem has shown from two to three phases.
- The numbers of linear and nonlinear iterations for both GMRES and ORTHOMIN increase nonlinearly with the number of unknowns, the linear iteration numbers are better for GMRES than for ORTHOMIN, particularly for problems of larger sizes, and the nonlinear iteration numbers are almost the same for both algorithms.

The numerical observations made in this paper agree with theory. All Krylov subspace algorithms are related to the choice of a basis of a Krylov subspace. In GMRES, an orthogonal basis of a Krylov subspace is used, while in ORTHOMIN, the search directions u_k are sought to be $A^{\mathrm{T}}A$-orthogonal in the same Krylov subspace. Both the set of the u_k's and that of the Au_k's need be stored in ORTHOMIN, which almost doubles the storage requirement compared with GMRES. The number of arithmetic operations per iteration is also roughly 50% higher than GMRES.

REFERENCES

1. Aziz K. Reservoir simulation grids: opportunities and problems. *The 12th SPE Symposium on Reservoir Simulation held in New Orleans*, SPE 25233, LA, U.S.A., February 28–March 3, 1993.
2. Heinrichs B. *Finite Difference Methods on Irregular Networks*. Birkhauser: Basel, Boston, Stuttgart, 1987.
3. Forsyth PA. A control volume finite element method for local mesh refinement. *The SPE Symposium on Reservoir Simulation in Houston*, SPE 18415, TX, February 6–8, 1989.
4. Fung LS, Hiebert AD, Nghiem L. Reservoir simulation with a control volume finite element method. *The 11th SPE Symposium on Reservoir Simulation*, SPE 21224, Anaheim, February 17–20, 1991.
5. Verma S, Aziz KA. Control volume scheme for flexible grids in reservoir simulation. *Paper SPE 37999*, *The 1997 SPE Symposium on Reservoir Simulation*, Dallas, June 8–11, 1997.
6. Li B, Chen Z, Huan G. Control volume function approximation methods and their applications to modeling porous media flow I: the two-phase flow. *Advances in Water Resources* 2003; **26**:435–444.
7. Li B, Chen Z, Huan G. Control volume function approximation methods and their applications to modeling porous media flow II: the black oil model. *Advances in Water Resources* 2004; **27**:99–120.
8. Vinsome PKW. ORTHOMIN, an iterative method for solving sparse sets of simultaneous linear equations. *Proceedings of the Fourth Symposium on Reservoir Simulations*, Society of Petroleum Engineers of AIME, 1976; 149–157.
9. Saad Y, Schultz MH. GMRES: a generalized minimal residual algorithm for solving nonsymmetric linear systems. *SIAM Journal on Scientific and Statistical Computing* 1986; **7**:856–869.
10. Choquet R, Erhel J. Newton-GMRES algorithm applied to compressible flows. *International Journal for Numerical Methods in Fluids* 1996; **23**:177–190.
11. Li W, Chen Z, Ewing RE, Huan G. Comparison of the GMRES and ORTHOMIN for the black oil model in porous media. *International Journal for Numerical Methods in Fluids* 2005; **48**:501–519.
12. Aziz K, Settari A. *Petroleum Reservoir Simulation*. Applied Science Publishers Ltd: London, 1979.
13. Chen Z, Huan G, Ma Y. *Computational Methods for Multiphase Flows in Porous Media*, Computational Science and Engineering Series, vol. 2. SIAM: Philadelphia, PA, 2006.
14. Peaceman DW. Interpretation of well-block pressures in numerical reservoir simulation. *52nd Annual Fall Technical Conference and Exhibition*, SPE 6893, Denver, 1977.
15. Saad Y. A flexible inner–outer preconditioned GMRES algorithm. *SIAM Journal on Scientific and Statistical Computing* 1993; **14**:461–469.
16. Golub GH, van Loan CF. *Matrix Computations*. Johns Hopkins University Press: Baltimore, London, 1983.
17. Chen Z, Li B, Huan G, Espin D, Klie H, Buitrago S. Control volume function approximation method for the black oil model. *Proceedings of the 2nd Meeting on Reservoir Simulation*, Universidad Argentina de la Empresa, Buenos Aires, Argentina, November 5–6, CD-ROM, 2002.
18. Origin 2000 and Onyx2 performance tuning and optimization guide. *SGI Document Number 007-3430-003*.
19. Odeh AS. Comparison of solutions to a three-dimensional black-oil reservoir simulation problem. *Journal of Petroleum Technology* 1981; 13–25.

